

A study on aeroelastic forces due to vortex-shedding by reduced frequency response function

Xin Zhang*

School of Civil Engineering, Zhengzhou University, Zhengzhou, China

Zhanying Qian, Zhen Chen and Fanna Zeng

Henan Provincial Agency of Quality Supervision for Construction Industry, Zhengzhou, China

(Received March 12, 2008, Accepted December 16, 2008)

Abstract. The vortex-induced vibration of an Γ -shaped bridge deck sectional model is studied in this paper via the wind tunnel experiment. The vibratory behavior of the model shows that there is a transition of the predominant vibration mode from the vertical to the rotational degree of freedom as the wind speed increases gradually or vice versa as the wind speed decreases gradually. The vertical vibration is, however, much weaker in the latter case than in the former. This is a phenomenon which is difficult to model by existing parametric models for vortex-induced vibrations. In order to characterize the aeroelastic property of the Γ -shaped sectional model, a time domain force identification scheme is proposed to identify the time history of the aeroelastic forces. After the application of the proposed method, the resultant fluid forces are re-sampled in dimensionless time domain so that reduced frequency response function (RFRF) can be obtained to explore the properties of the vortex-induced wind forces in reduced frequency domain. The RFRF model is proven effective to characterize the correlation between the wind forces and bridge deck motions, thus can explain the aeroelastic behavior of the Γ -shaped sectional model.

Keywords: force identification; bridge deck sectional model and vortex-shedding.

1. Introduction

Vortex-shedding is an interesting phenomenon that happens to bluff bodies. It becomes the major concern when the structure, such as the deck of cable supported bridges, is flexible and damped very lightly.

The general problem of vortex-induced vibration has been subjected to intensive studies. Early researchers, such as Iwan and Blevins (1974) and Billah (1989) developed wake-body-coupled models in which the body oscillation and wake oscillation are coupled through interaction terms. Other researchers such as Chen, *et al.* (1995), Ehsan and Scanlan (1990) and Gupta, *et al.* (1996), utilized single dynamic equation with aeroelastic terms, which can be identified by experiments.

Experimental studies on fluctuating wind forces on prisms with various sectional properties are

* Associate Professor, Corresponding Author, E-mail: 146719464@ntu.edu.sg

plenty. Kim and Sakamoto (2006) used forcing devices to “reproduce” the free vibration of a circular cylinder in the cross-flow direction and measure the fluctuating lift forces to investigate, among other issues, the work done by the fluctuating lift force and the phase between the body motion and fluid force. It was reported that the phase between the fluctuating lift force and the cylinder displacement changes abruptly as the reduced velocity increases. Takai and Sakamoto (2006) studied torsional vibrations of rectangular prisms and classified the vibration into six patterns depending on the width-to-depth ratio. For more complex cross sections, Choi and Kwon (2003) studied the effect of corner cuts on the Strouhal number of rectangular cylinders with various dimensional ratios and various angles of attack. The test results show that the Strouhal number of the model with various corner cuts has a fluctuating trend as the angle of attack changes. For each cutting ratio as the angle of attack increases at cutting ratio above 15° , the Strouhal number decreases gradually, and these trends are more evident for larger corner cut sizes. Experimental studies are also reported by Cheng and Tanaka (2005), Tamura and Dias (2003) Itoh and Tamura (2002), Leonard and Roshko (2001), Mills, *et al.* (2003) and others.

It can be inferred from the literatures reviewed above that many of the current studies on vortex-induced force on prism structures are based on indirect measurements of the fluid force. It would be useful if the fluid force can be identified directly from the response of the oscillating body, and the properties of the aeroelastic system can be investigated by direct relating the fluid force time history with the body motion time history. It is particularly the case when complex patterned vortex-shedding exists as what has happened to the Sectional model studied in this paper.

2. The sectional model

The bridge deck model (Fig. 1) studied in this paper is excited by the motion-induced vortices, which are generated at the leading edge of the girder. At low wind speed, the flow separates from the leading edge and reattaches to the sectional model. Because the lower surface of the model is open, exposing the transversal and axial girders to the reattached wind flow, complex flow pattern is generated. As wind speed increases from 2.5 to 4.0 m/s, the reattachment point moves downstream, finally, the flow does not re-attach. During this process, the model experiences a transition of the predominant vibration mode from the vertical to the rotational degree of freedom.

The transition of the predominant vibration mode indicates the bifurcation of the bridge behavior in a time-varying wind speed environment: the vibration could switch between vertical and rotational degree of freedom due to small change of the mean wind speed. The frequency ratio of the vertical and rotational vibration (3.3 Hz /5.3 Hz) was designed to match the frequency ratio of the prototype. Therefore the transition of the predominant vibration mode is considered as the inherent characteristic of the problem that can not be bypassed by setting the frequency ratio to a different value. A

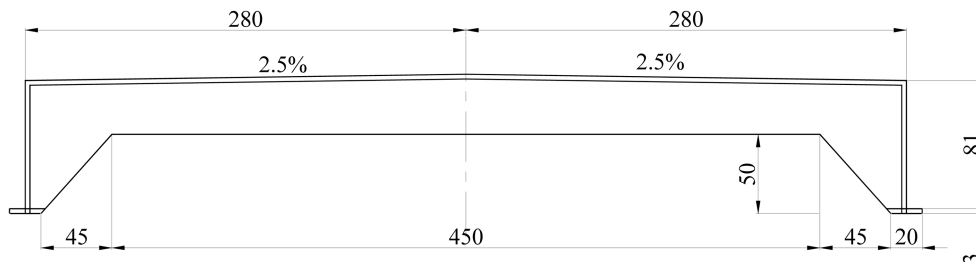


Fig. 1 The Sectional Model (Dimension in mm)

theoretical explanation of this phenomenon might be complex and it is beyond the scope of this research, which would rather focus on “curve fitting” instead of explaining the phenomenon.

In this case, it would be easier to identify the dynamic wind forces directly to obtain the frequency domain properties of the wind forces, i.e. to find a linearized mapping between the bridge deck motion and the aerodynamic forces: $f(K) = H(K)x(K)$, where $f(K)$ is the dynamic wind forces in reduced frequency, K , domain; $H(K)$ is the reduced frequency response function (RFRF) and $x(K)$ is the displacement of the structure in reduced frequency domain.

Therefore, the objective of this paper is to propose a method for the direct identification of the aerodynamic forces so that the above mentioned reduced frequency response function can be computed. For the sake of completeness, the RFRF is identified for both wind speed increasing and decreasing cases.

3. Method for the identification of dynamic wind forces

For a two-dimensional sectional model with degrees of freedom in vertical and rotational direction, the vibration equation can be written as:

$$\begin{aligned} \dot{X}(t) &= A_c X(t) + B_c f(t) \\ Y(t) &= C X(t) + D f(t) \end{aligned} \quad (1)$$

where $X(t) = \{x^T(t), \dot{x}^T(t)\}^T$ is the state variable;

$$A_c = \begin{bmatrix} 0 & I \\ -M^{-1}K_m & -M^{-1}C_m \end{bmatrix} \quad (2)$$

is the state matrix; $B_c = \begin{bmatrix} 0 \\ M^{-1} \end{bmatrix}$ is the input matrix;

$C = [C_d - C_a M^{-1}K \quad C_v - C_a M^{-1}C_m]$ is the output matrix; $D = C_a M^{-1}$ is the feed through due to the measurement of acceleration and $f(t) = \begin{Bmatrix} F_h \\ F_a \end{Bmatrix}$, the wind force vector.

In the expressions above, $x(t) = \{h(t), \alpha(t)\}^T$ is the displacement time history vector comprising of vertical displacement, $h(t)$, and rotational displacement, $\alpha(t)$; M is the mass matrix of the model, K_m and C_m are the stiffness and damping matrix respectively; C_d C_v C_a are the influence factor for displacement, velocity and acceleration measurement respectively; $F_h(t)$ is the lifting force and $F_a(t)$ is the rotational moment.

In this study, only displacement is measured, therefore, $C = \begin{bmatrix} 1 & 0 & 0 & 0 \\ 0 & 1 & 0 & 0 \end{bmatrix}$ and D is a null matrix.

In the equation, all the wind forces, including the vortex-shedding forces, have been put into the force vector $f(t)$, so that the state matrix is purely structural.

In discrete time format, the same system above is:

$$\begin{aligned} X(i+1) &= AX(i) + Bf(i) \\ Y(i) &= CX(i), \end{aligned} \quad (3)$$

Where

$$\begin{aligned} A &= e^{A_c \Delta t} \quad \text{and} \\ B &= \int_0^{\Delta t} e^{A_c \tau} B_c d\tau. \end{aligned} \quad (4)$$

in the equation, $i = 0, 1, 2, \dots, n$ indicates the sequence of the sampled data.

To perform the computation using displacement time history only, a similarity transform is performed, i.e. use $X^* = TX$ as a new state vector, where $T = \begin{bmatrix} C \\ CA \end{bmatrix}$ is the transform matrix.

After the transform, the discrete state space equation is

$$\begin{aligned} X^*(i+1) &= A^* X^*(i) + B^* f(i) \\ Y(i) &= C^* X^*(i) \end{aligned} \quad (5)$$

where, $A^* = TAT^{-1}$, $B^* = TB$ and $C^* = CT^{-1}$. The state vector is $X^*(i) = TX = \begin{Bmatrix} x(i) \\ z(i) \end{Bmatrix}$, where $x(i)$ is the discrete measurement of displacement and $z(i)$ is a variable containing a force term.

The structure of matrix A^* can be certified to be in the form of (Jakobsen and Hansen; 1995)

$$A^* = \begin{bmatrix} 0 & I \\ -[a_0] & -[a_1] \end{bmatrix} \quad (6)$$

and the output matrix $C^* = \begin{bmatrix} 1 & 0 & 0 & 0 \\ 0 & 1 & 0 & 0 \end{bmatrix}$.

Substituting A^* , B^* and C^* into Eq. (5) leads to

$$[I \ [a_1] \ [a_0]] \begin{Bmatrix} x(k+2) \\ x(k+1) \\ x(k) \end{Bmatrix} = [b_1 \ b_0] \begin{Bmatrix} f(k+1) \\ f(k) \end{Bmatrix} \quad (7)$$

where $[b_1] = [I \ 0]B^*$ and $[b_0] = [[a_1] \ I]B^*$.

This equation describes an autoregressive model with external input (ARX), whose parameters, $[b_0]$, $[b_1]$, are predefined by the autoregressive parameters $[a_0]$, $[a_1]$. The autoregressive coefficient matrix can be identified directly from the free vibration of the sectional model under no-wind condition with an AR model.

If $k+2$ measurements are available, Eq. (7) becomes

$$[I \ [a_1] \ [a_0]] \begin{Bmatrix} x(3) \ x(4) \ \cdots \ x(k+2) \\ x(2) \ x(3) \ \cdots \ x(k+1) \\ x(1) \ x(2) \ \cdots \ x(k) \end{Bmatrix} = [b_1 \ b_0] \begin{Bmatrix} f(2) \ f(3) \ \cdots \ f(k+1) \\ f(1) \ f(2) \ \cdots \ f(k) \end{Bmatrix}. \quad (8)$$

where $x(i) = \begin{Bmatrix} h(i) \\ \alpha(i) \end{Bmatrix}$, ($i = 1, \dots, k+2$) are the displacement time history measurements.

Multiplying Eq. (8) by a pseudo-inverse of matrix $[b_1 \ b_0]$, the wind force is estimated in the least squares sense:

$$\begin{Bmatrix} f(2) & f(3) & \cdots & f(k+1) \\ f(1) & f(2) & \cdots & f(k) \end{Bmatrix} = [b_1 \ b_0]^+ [I \ [a_1] \ [a_0]] \begin{Bmatrix} x(3) & x(4) & \cdots & x(k+2) \\ x(2) & x(3) & \cdots & x(k+1) \\ x(1) & x(2) & \cdots & x(k) \end{Bmatrix}, \quad (9)$$

where $[b_1 \ b_0]^+$ is the pseudo inverse of $[b_1 \ b_0]$ so that $[b_1 \ b_0]^+ [b_1 \ b_0] = I$. Eq. (9) offers one set of the possible force time histories that can drive the model to vibrate in the recorded way.

4. Identification of reduced frequency response function (RFRF) for the wind forces

The identified wind forces are random processes with predominant frequencies. The effect of such forces is affected by factors such as the instantaneous phase angle between the wind force and the model displacement. The distribution of the random phase angle is thus important in understanding the response of the model. This information can be obtained by introducing the wind force reduced frequency response function (RFRF).

$$H(K) = \frac{f(K)}{x(K)}, \quad (10)$$

where K is reduced frequency; the complex valued $H(K)$ is the response function in reduced frequency domain; $x(K)$ and $f(K)$ are Fourier transformed displacement and wind forces in reduced frequency domain, respectively.

Noted is that the fluid is the system to be identified with model displacement as the input. The absolute value of $H(K)$ reflects the magnitude of the wind forces activated by unit displacement at reduced frequency K . The phase angle of $H(K)$ indicates the wind forces are leading ahead or lagging behind the model motion.

In extracting the reduced frequency response function, a chirp signal of the input term, i.e. the body displacement time history with continuously changing frequencies, is preferred so that a fine resolution of the RFRF is possible. While the frequency of the free vibration is not changeable, a chirp signal can be obtained in dimensionless time domain by controlling the mean wind speed to vary at a very low changing rate.

When there is continuously changing wind speed, the interval of the dimensionless time is defined as

$$\Delta S = \frac{\bar{U}(t)}{B} \Delta t, \quad (11)$$

where ΔS is the interval of dimensionless time S , $\bar{U}(t)$ is the positive instantaneous average value of wind speed over time step Δt centered around time t and B is the deck width.

Thus, the dimensionless time may be defined by

$$S = \int_{t_0}^t \frac{\bar{U}(t)}{B} dt \quad (12)$$

The estimated wind forces, together with the displacement time history, can then be transferred to dimensionless time domain, i.e. $f(S)$ and $x(S)$, and re-sampled at even sampling rate in dimensionless time domain. By adjusting the wind speed gradually for U_1 at time t_0 to U_2 at time t , we change the

reduced frequency from $K_1 = \frac{nB}{U_1}$ to $K_2 = \frac{nB}{U_2}$, where n is the body oscillation frequency.

If the lock-in reduced frequencies fall between K_1 and K_2 , the frequency response function of the vortex-shedding forces can be expressed in reduced frequency domain as shown in Eq. (10).

5. The experiments and results

As shown in Fig. 2, the model was suspended by eight springs to allow for vertical and rotation free vibration. The lateral motion was restrained by thin wire. The spring constant and the spring anchorage point were so chosen such that they have a combined stiffness producing the vertical frequency of 3.3 Hz and the rotation frequency 5.3 Hz. Two laser displacement sensors were installed below the front and rear edge of the model to record the vertical and rotational displacement. The sampling frequency was 50 Hz. One hotwire anemometer was installed in front of the model to record the horizontal wind speed. No turbulence generating device was used. The typical turbulence intensity is less than 2 percent. Therefore, the oncoming wind was considered smooth.

The testing program was performed in two steps: the structural parameters under no-wind condition were identified first by triggered free decay vibration and $[a_0]$, $[a_1]$ and $[b_0]$, $[b_1]$ were obtained; the response of the sectional model when the smooth wind flow was applied was then recorded. The wind changed from higher wind speed to lower wind speed monotonously and then ramp up to a higher wind speed, covering the wind speed range of interest. The changing rate of the wind speed was controlled to be as slow as 1m/s/500s, to allow full development of the vortex-shedding response.

As is shown in Fig. 3, due to the special cross section shape, the model is active both in the vertical and rotation direction within the wind speed region between 2 to 4 m/s due to the vortex-shedding excitation. Measurements of the dynamic wind forces on the fixed model by force transducers show Strouhal Numbers of 0.85 for vertical motion dominant period and 0.79 for the rotational motion dominant period. (The Strouhal number is computed as $S_t = N_s D / U$ where N_s is the vortex-shedding frequency D is the characteristic dimension of the model and U wind speed)

It can be observed that in the wind speed decreasing case, the vortex-shedding locks onto the

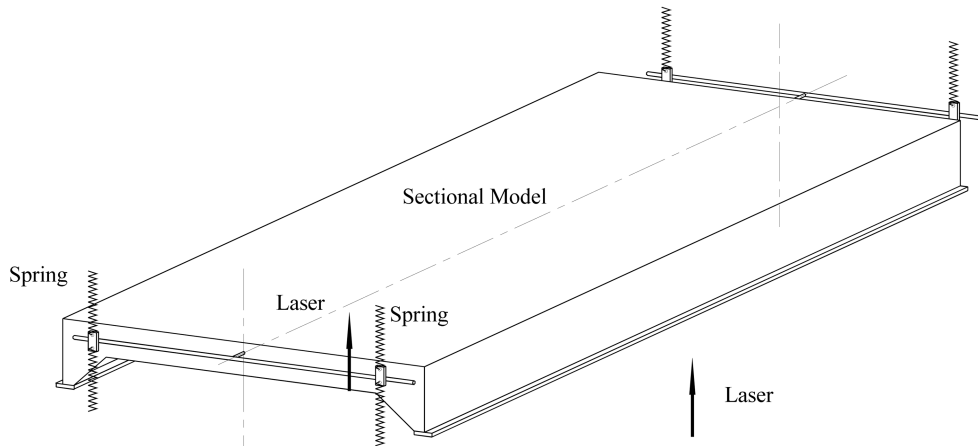


Fig. 2 The Suspension System

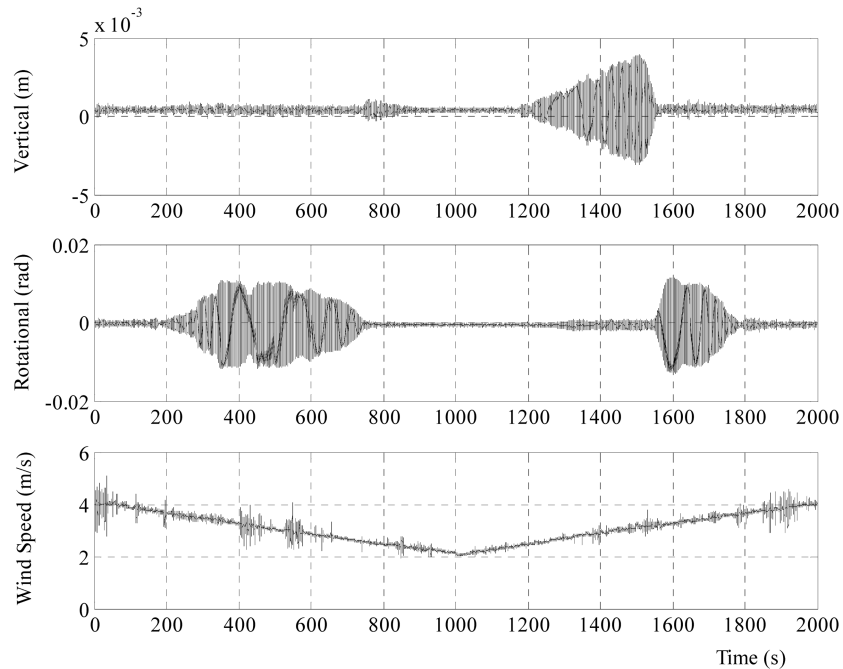


Fig. 3 Displacements and Wind Speed vs. Time

rotational motion first and sticks to the rotation motion, showing a roughly symmetric amplitude envelope. The lock-in in the vertical motion is suppressed, with only weak signs of existence after the rotational lock-in region has passed. In the wind speed increasing case, however, the vortex-shedding locks onto the vertical motion first and then comes to a sudden stop, giving way to the lock-in in the rotational direction. The rotational lock-in then becomes predominant. Both the vertical and rotational amplitude envelopes are not symmetric in this case.

In order to have a better understanding of the data, the proposed force identification method is applied. In the analysis, the wind forces are identified for wind speed decreasing case and increasing case separately to avoid confusion of the data in reduced frequency domain. In the analysis, the data was de-noised before the force identification is performed by using the wavelet decomposition which has good performance in maintaining the original phase relations.

To test the effectiveness of the proposed method, a comparison study was performed. A segment of measured displacement time history in Fig. 3 between 1200s-1500s was subjected to the proposed procedure to identify the force vector, which was subsequently used as the driven force on the same numerical model to produce the reconstructed response signal. A segment of results are shown in Fig. 4. It can be seen that the discrepancies between the two signals are acceptably small. Therefore the force identification method proposed in the paper works reasonably well.

6. The wind speed increasing case

The identified wind forces for the wind speed increasing case are shown in Fig. 5. As expected, in an operational environment, the estimated input forces of a dynamic system should contain noise. However, the prediction errors are usually wide banded in frequency domain. Therefore, if the result

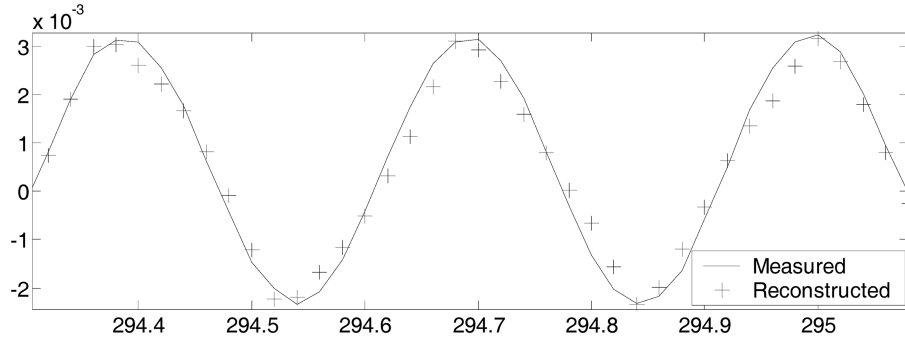


Fig. 4 The Measured and Reconstructed Signal Driven by the Identified Force

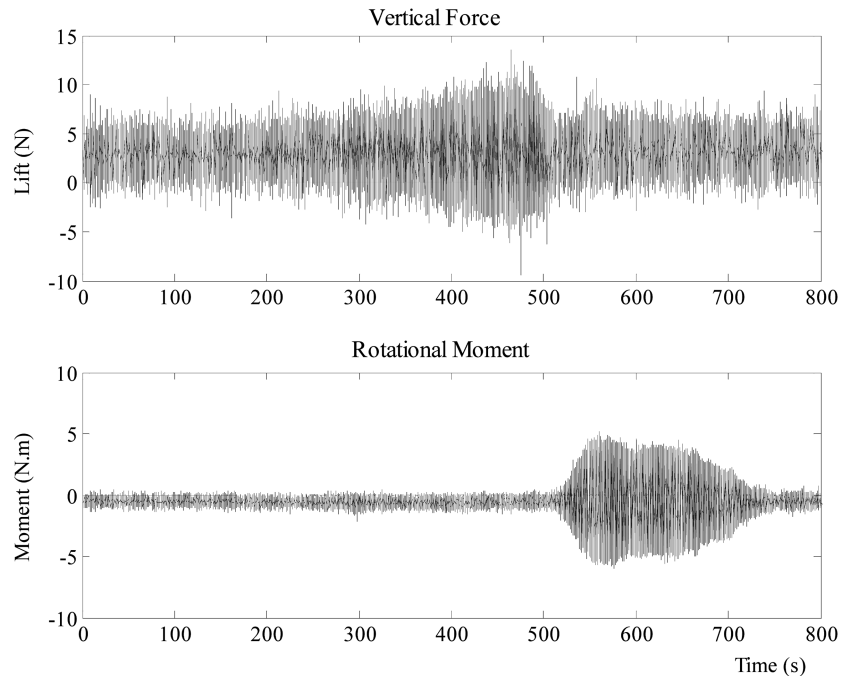


Fig. 5 Identified Wind Forces (Wind Speed Increasing Case)

is used in frequency domain instead of time domain, it would be more reliable as meaningful part of the signal may be concentrated in a narrower frequency band while the errors spread over a wider frequency band, resulting in a low intensity of energy.

The fast Fourier transform (FFT) result of the identified forces in reduced frequency domain are shown in Fig. 6. It can be seen that the lifting force has two major reduced frequency bands. One is around 0.6 (dimensionless) and the other falls between 0.83 to 0.93. The vertical response of the model mainly concentrates between 0.58 to 0.7, matching the lower frequency center of the lifting force. The rotational moment also has two peaks covering from 0.58 to 0.7 and from 0.83 to 0.93. The rotational displacement shows predominant frequency between 0.83 to 0.93. Very weak responses exist around 0.6.

These observations might suggest that the rotational moment at the lower frequency region is

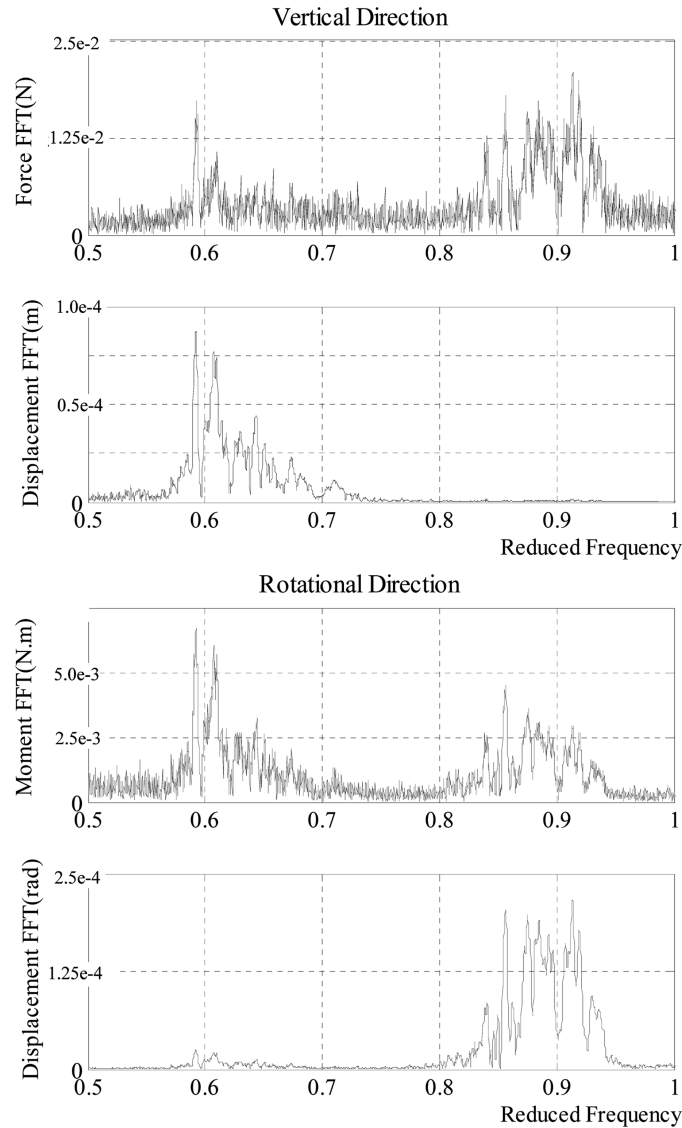


Fig. 6 FFT of Displacements and Wind Forces in Reduced Frequency Domain (Wind Speed Increasing Case)

generated by the vertical movement and the lifting force at the higher frequency is related to the rotational motion.

The phase angle of the RFRF is shown in Fig. 7. In the figure, “A” represents rotation direction; “H” denotes vertical direction; “AH” denotes the rotational moment due to displacement in the vertical direction. The phase angle of AH is the angle by which the rotation moment leads the vertical displacement. “AA, HH, HA” are defined in the similar way.

Because the wind forces are random processes with predominant frequencies, the phase angles show dispersals. However, these figures do show concentrations of phase angle within upper and lower lock-in region.

From reduced frequency 0.58 to 0.7, the rotational moment slightly lags behind the rotational

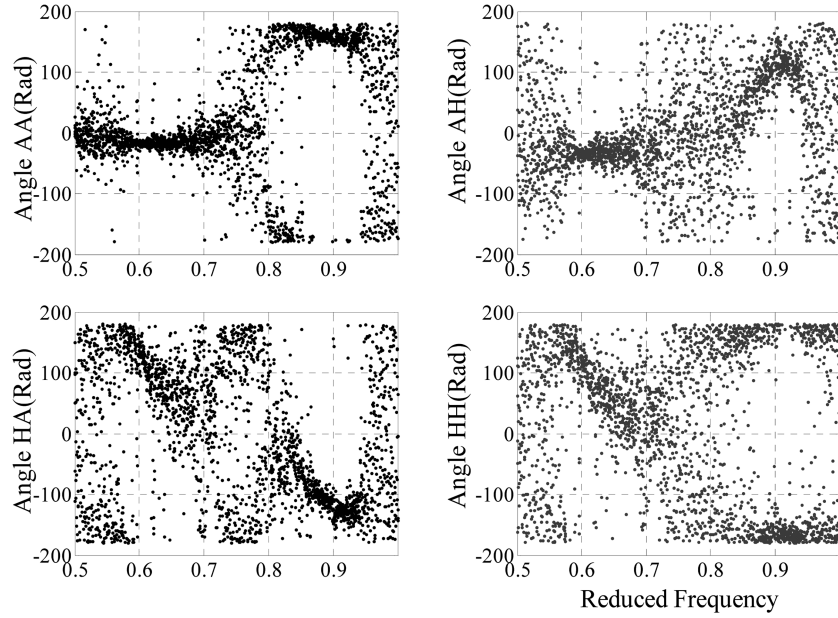


Fig. 7 Phase Angle between the Wind Force and the Model Displacement (Wind Speed Increasing Case)

displacement (Angle AA), whose effect is positive damping and negative stiffness (be noted the minus signs in matrix A_c of Eq. (2)). Therefore, even the rotational moment is large within this region, the model response remains small. In the plot “HH”, there is a migration of the phase angle from 180° to 0° , generating negative aeroelastic damping. The vertical motion predominates due to smaller effective vertical damping. It is also observed in plot “AH”, the correlation between the rotational moment and vertical displacement is clear, suggesting the aeroelastic coupling between rotational and vertical direction.

From reduced frequency 0.8 to 0.93, the rotational moment is always leading the rotational displacement by an angle slightly less than 180° (Angle AA) reducing the effective rotational damping. Therefore, rotational response becomes the major response within this region. On the other hand,

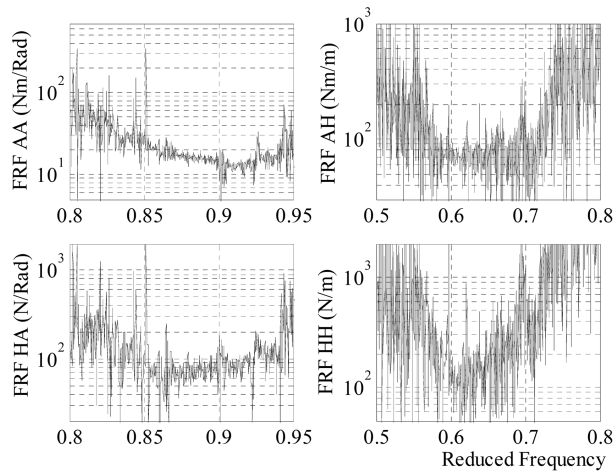


Fig. 8 Absolute Value of the FRFs of Wind Forces (Wind Speed Increasing Case)

the phase angles between lifting force and vertical motion (Angle HH) are symmetrically distributed around 180^0 . The wind force contributes to positive stiffness. The vertical motion is, therefore, small. The aeroelastic coupling at this reduced frequency is still clear (Angle HA), indicating the lifting force is generated by the rotational motion.

Between 0.7 and 0.8, there is a transition region in the subplot AA and HH. The phase angles are distributed symmetrically (or almost so) around zero line causing a cancellation of the aeroelastic effects. This corresponds to the transition period between 1500s and 1600s in Fig. 3.

In Fig. 8, the absolute values of the wind force RFRF are shown at the reduced frequencies where the denominator in Eq. (10) is large. The conventions of this figure are the same as Fig. 7.

7. The wind speed decreasing case

The identified wind forces are shown in Fig. 9. The reduced frequency representations are shown in Fig. 10. It is noticed that the magnitude of the FFT of vertical displacement is considerably lower than the same parameter in the wind speed increasing case. The figures show there is lifting force at the reduced frequency of the rotational movement due to the aeroelastic coupling effect. The lifting force, however, generates weak vertical response at this frequency. The phase angle between the lifting force and vertical motion is shown in Fig. 11, subplot Angle HH. Around the reduced frequency of 1, where the lifting force is active, the vertical displacement leads the force by an angle less than 180^0 , hence the model is experiencing positive aeroelastic damping and aeroelastic stiffness. The vertical displacement is damped out.

The aeroelastic coupling is indicated in the subplot Angle HA. From 0.8 to 1, the phase angle between the lifting force and rotational displacement continuously change from 0^0 to an angle slightly less than 180^0 , and stay constant until 1.2 is reached, indicating the coupling term is changing from displacement related to velocity related and then changing to displacement related again. In the

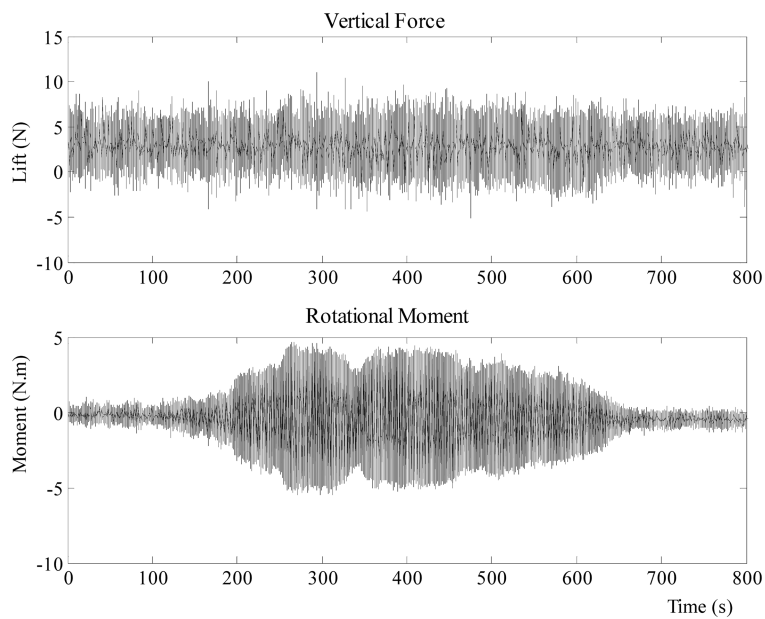


Fig. 9 Identified Wind Forces (Wind Speed Decreasing Case)

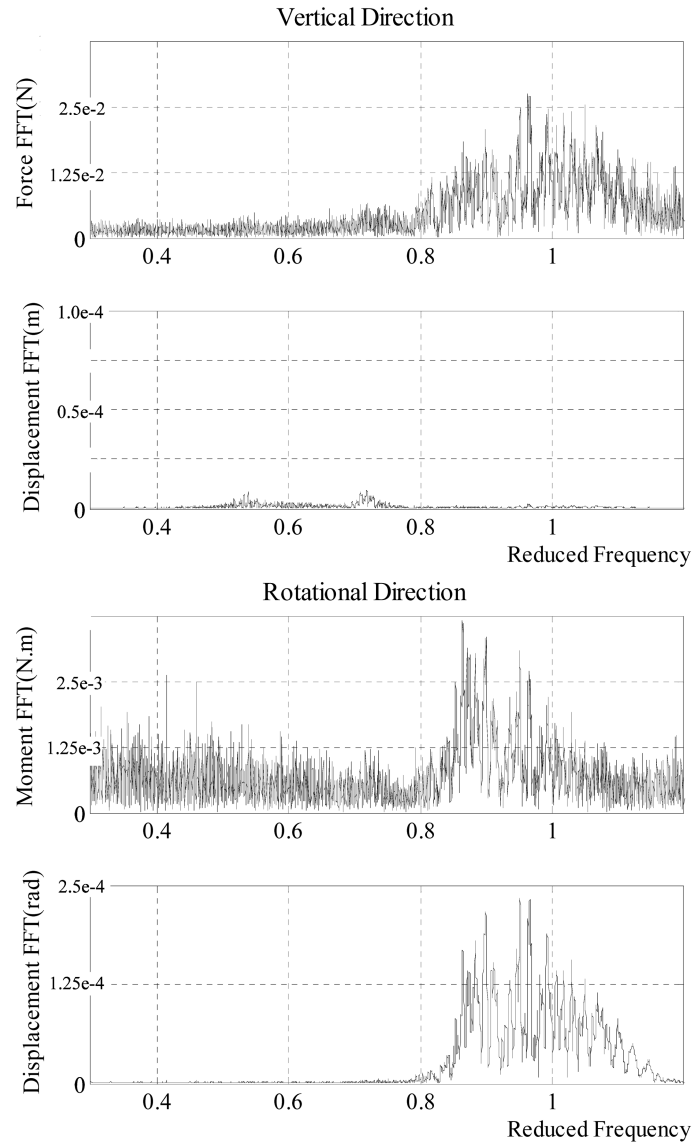


Fig. 10 FFT of the Wind Forces in Reduced Frequency Domain (Wind Speed Decreasing Case)

rotational direction, the situation is similar to the previous case, except for the distribution of the phase angle is more scattered.

In Fig. 12, the absolute value of RFRF AA and HA are shown at the rotational lock-in region. The value of RFRF AA, to certain accuracy, is in consistence with the former case despite the large noise component. So is the value of RFRF HA.

8. Conclusions

The aeroelastic effects of the complex patterned vortex shedding from a sectional model of Π -

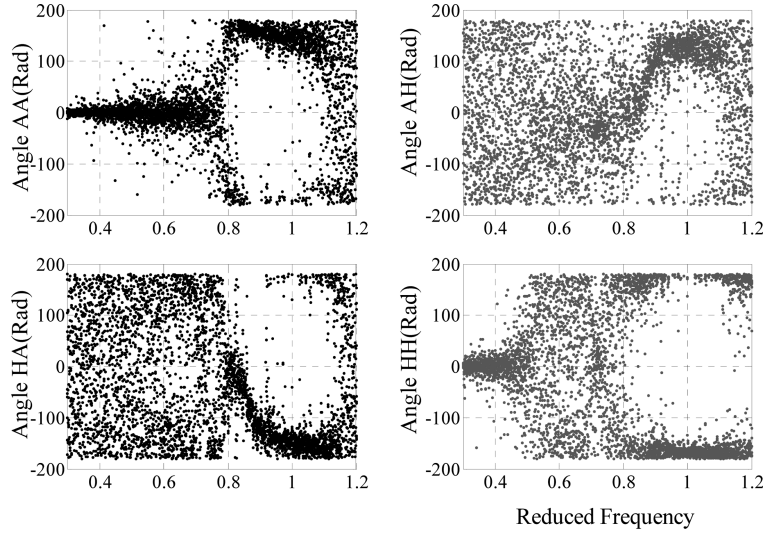


Fig. 11 Phase Angle between the Wind Forces and the Model Displacement (Wind Speed Decreasing Case)

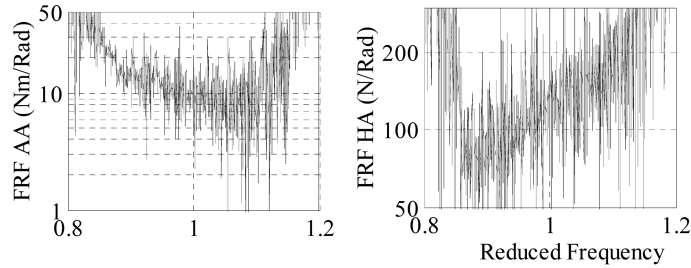


Fig. 12 Absolute Value of FRFs of Wind Forces (Wind Speed Decreasing Case)

shape are successfully studied by the proposed reduced frequency response function. This RFRF model is realized through a time domain identification scheme for aerodynamic forces due to wind with slow monotonously increasing or decreasing speed and may serve as an alternative to the existing methods when the vortex shedding pattern is too complex to be described by a parametric model. The beauty of the proposed method is that it can clearly picture the linearized mapping relation between the displacements and aerodynamic forces. Through the proposed method, strong aerodynamic coupling effect between the vertical and rotational motion of the bridge is discovered; aeroelastic features of the bridge are explained by the phase of the RFRF giving insights into whether the aeroelastic effect is damping related or stiffness related.

Nomenclature

- $[a_0], [a_1]$: Coefficient matrices
- A, A^*, A_c : State matrices
- $[b_0], [b_1]$: Coefficient matrices
- B, B^*, B_c : Input Matrices
- C, C^* : Output matrices

C_d, C_v, C_a	: Measurement influence factor
C_m	: Structural damping matrix of the model
D	: Feed through matrices
$f(t), f(i), f(K)$: Wind force
$h(t), h(i)$: Vertical displacement
$H(K)$: Frequency response function of wind force
i, k	: Indices
K	: Reduced Frequency
K_m	: Structural stiffness matrix of the model
S	: Dimensionless time
T	: Transform matrix
$\bar{U}(t)$: Instantaneous averaging wind speed
$x(t), x(i), x(K)$: Displacement vectors
$X(t), X(i), X^*(i)$: State vectors
$Y(t), Y(i)$: Output measurements
$\alpha(t), \alpha(i)$: Rotational displacement

References

- Billah, K.Y.R. (1989), "A study of vortex-induced vibration", Ph.D. dissertation, Princeton University, Princeton, N.J.
- Chen, S.S., Zhu, S. and Cal, Y. (1995), "An unsteady flow theory for vortex-induced vibration", *J Sound Vib.*, **184**(1), 73-92.
- Cheng, S. and Tanaka, H. (2005), "Correlation of aerodynamic forces on an inclined circular cylinder", *Wind Struct.*, **8**(2), 135-146.
- Choi, C.K. and Kwon, D.K. (2003), "Effects of corner cuts and angles of attack on the Strouhal number of rectangular cylinders", *Wind Struct.*, **6**(2), 127.
- Ehsan, F. and Scanlan, R.H. (1990), "Vortex-induced vibration of flexible bridges", *J. Eng. Mech.*, ASCE, **116**(6), 1392-1411.
- Gupta, H., Sarkar, P.P. and Mehta, K.C. (1996), "Identification of vortex-induced response parameters in time domain", *J. Eng. Mech.*, ASCE, **122**(11), 1031-1037.
- Itoh, Y. and Tamura, T. (2002), "The role of separated shear layers in unstable oscillations of a rectangular cylinder around a resonant velocity", *J. Wind Eng. Ind. Aerod.*, **90**, 377-394.
- Iwan, W.D. and Blevins, R.D. (1974), "A model for vortex-induced oscillations of structures", *J. Appl. Mech.*, **41**(3), 581-586.
- Jakobsen, J.B. and Hansen, E. (1995), "Determination of Aerodynamic Derivatives by a System Identification Method", *J. Wind Eng. Ind. Aerod.*, **57**, 295-305.
- Kim, S. and Sakamoto, H. (2006), "Characteristics of fluctuating lift forces of a circular cylinder during generation of vortex excitation", *Wind Struct.*, **9**(2), 109-124.
- Leonard, A. and Roshko, A. (2001), "Aspects of flow-induced vibration", *J. Fluids Struct.*, **15**, 415-425.
- Mills, R., Sheridan, J. and Hourigan, K. (2003), "Particle image velocimetry and visualization of natural and forced flow around rectangular cylinders", *J. Fluid Mech.*, **478**, 299-323.
- Takai, K. and Sakamoto, H. (2006), "Response characteristics and suppression of torsional vibration of rectangular prisms with various width-to-depth ratios", *Wind Struct.*, **9**(1), 1.
- Tamura, T. and Dias, P.P.N.L. (2003), "Unstable aerodynamic phenomena around the resonant velocity of a rectangular cylinder with small side ratio", *J. Wind Eng. Ind. Aerod.*, **91**, 127-138.